ARTICLE

Synthesis and Characterisation of Biocompatible Organic-Inorganic Core-Shell Nanocomposite Particles based on Ureasils

Received 00th January 20xx,
Accepted 00th January 20xx

DOI: 10.1039/x0xx00000x

Ilaria Meazzini[a,b]†, Steve Comby[b]†, Kieran D. Richards[a], Aimee M. Withers[c], François-Xavier Turquet[b‡], Judith E. Houston[b§], Róisín M. Owens[c] and Rachel C. Evans[a]*

Organic-inorganic core-shell nanocomposites have attracted increasing attention for applications in imaging, controlled release, biomedical scaffolds and self-healing materials. While tunable properties can readily be achieved through the selection of complementary building blocks, synergistic enhancement requires management of the core-shell interface. In this work, we report a facile one-pot method to fabricate hybrid core-shell nanocomposite particles (CSNPs) based on ureasils. The native structure of ureasils, which are poly(oxyalkylene)/siloxane hybrids, affords formation of an organic polymer core via nanoprecipitation, while the terminal siloxane groups act as a template for nucleation and growth of the silica shell via the Stöber process. Through optimisation of the reaction conditions, we demonstrate the reproducible synthesis of ureasil CSNPs, with a hydrodynamic diameter of ~150 nm and polydispersity <0.2, which remain electrostatically stabilised in aqueous media for >50 days. Selective functionalisation, either through the physical entrapment of polarity-sensitive fluorescent probes (coumarin 153, pyrene) or covalent-grafting to the silica shell (fluorescein isothiocyanate) is also demonstrated and provides insight into the internal environment of the particles. Moreover, preliminary studies using a live/dead cell assay indicate that ureasil CSNPs do not display cytotoxicity. Given the facile fabrication method and the structural tunability and biocompatability of the ureasils, this approach presents an efficient route to multifunctional core-shell nanocomposite particles whose properties may be enhanced and tailored for a targeted application.

Introduction

Organic-inorganic hybrids prepared using sol-gel chemistry offer a versatile route to multifunctional materials whose shape, form and properties can be easily tuned based on the combination of different building blocks.[1,2] In particular, core-shell nanocomposite particles (CSNPs) offer the advantage of distinct segregation of organic and inorganic phases with complementary properties, whilst simultaneously presenting the opportunity for synergistic interactions at the phase interface that may lead to emergent properties.[3] Additional functionality can be introduced through the encapsulation of active species within the particle structure, e.g. fluorophores[4–8], stimuli-responsive molecules[9,10], or active pharmaceutical ingredients.[11–13] Moreover, with appropriate surface modification, CSNPs can be well-dispersed through an external medium (e.g. an emulsion[14] or polymer host[15,16]), which affords hierarchal control over the properties.

Among the vast possible combinations of materials, polymer-silica composite core-shell particles have attracted particular attention for their diverse potential applications, e.g. in sensing[17], imaging,[18] self-healing materials.[19–21] A polymer core offers a tunable chemical environment, which is advantageous for encapsulation, swelling and controlled release.[9,20,22] Similarly, silica is an attractive shell material, being robust, biocompatible and non-toxic.[23] The low isoelectric point of silica renders the surface negatively charged at pH>2, which facilitates electrostatic stabilization of their aqueous colloidal dispersions.[23]

A key challenge in the design of new CSNPs is that the core phase must provide a suitable template for shell deposition.[24] Depending on the synthetic process, this requires either surface modification of the core with an organosilane coupling agent (Stöber[25] route)[2] or the use of surfactants (microemulsion route).[24] Both methods increase the synthetic complexity and may lead to unwanted residual components that affect the colloidal stability. An alternative approach is to use an organic polymer core that is pre-functionalised with organosilane group to facilitate seamless nucleation and growth of the silica shell.[6] In previous studies, we, and others, have investigated a family of organic-inorganic hybrid

[a] Department of Materials Science & Metallurgy, University of Cambridge, 27 Charles Babbage Road, Cambridge, CB3 0FS, UK. Corresponding author: rce26@cam.ac.uk
[b] School of Chemistry, Trinity College Dublin, Dublin 2, Ireland
[c] Department of Chemical Engineering & Biotechnology, University of Cambridge, Philippa Fawcett Drive, Cambridge, CB3 0AS, UK.
† These authors contributed equally to this work.
‡ Present address : Laboratoire de Chimie, ENS Lyon, 46, allée d'Italie, 69364 LYON CEDEX 07, France
§ Present address: European Spallation Source ERIC, Box 176, SE-221 00 Lund, Sweden.
Electronic Supplementary Information (ESI) available: FTIR spectra of d-UPTES, detailed synthetic conditions for sample preparation, additional DLS data from size and stability studies, fluorescence decay curves and fitting data. See DOI: 10.1039/x0xx00000x

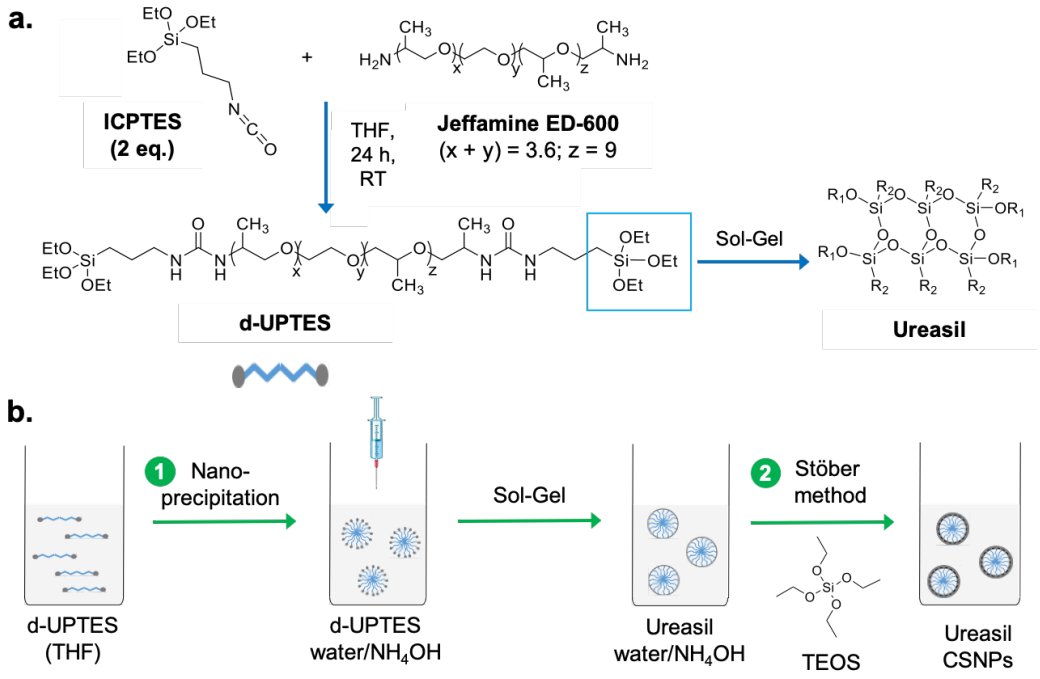

Figure 1. General synthetic route for the preparation of ureasil core-shell nanoparticles (CSNPs). (a) Reaction scheme for the synthesis of the d-UPTES organic-inorganic hybrid precursor and (b) schematic representation of the combined nanoprecipitation and Stöber processes used to obtain ureasil CSNPs.

materials known as *ureasils* as functional hosts for diverse applications including luminescent solar concentrators,[26–29] visible light communications[30] and electrochromic devices.[31]

Ureasils comprise a siliceous skeleton that is chemically-grafted to poly(oxyalkylene) chains via urea [NHC(=O)HN] bridges. Luminescent species can be readily incorporated into ureasils, by either chemical grafting[32,33] or entrapment.[26,34,35] They are most typically studied as transparent free-standing monoliths[36,37] or as thin films or coatings.[29,30] However, to the best of our knowledge, to date, ureasils have not been used for the synthesis of CSNPs, despite presenting the advantage of an intrinsic intermediate unit, namely di-ureapropyltriethoxysilane (d-UPTES, Figure 1), that can be used to seed the organic core of the particles, whilst simultaneously providing triethoxysilane terminal groups to facilitate nucleation and growth of the silica shell. Moreover, the d-UPTES structure can be readily tuned by varying the structure of the polyether amine precursor (Jeffamine ED-600 the present study, Figure 1), which enables tuning of the mechanical and chemical properties of the core structure.[32]

Based on this realisation, here we report a convenient liquid phase method to fabricate organic-inorganic composite CSNPs based on ureasils. Through optimization of the synthetic procedure, we demonstrate that ureasil CSNPs with enhanced colloidal stability (>50 days) can be prepared. The encapsulation of fluorescent dyes, by both physical entrapment and chemical grafting methods, is used to explore the internal chemical environment of the CSNPs, and also introduces the prospect of potential applications in imaging or sensing. Moreover, preliminary studies using a live/dead cell assay indicate that ureasil CSNPs do not display cytotoxicity.

Experimental

Reagents and Materials

O, O'-bis(2-aminopropyl)polypropylene glycol–*block*–polyethylene glycol-*block*–polypropylene glycol (Jeffamine ED-600), 3-(triethoxysilyl)propyl isocyanate (ICPTES, 95%), tetraethylorthosilicate (TEOS, ≥ 99%), ammonium hydroxide (NH_4OH, 5.01 N solution), Ludox solution (40%$_{w/w}$ in water), (3-aminopropyl)triethoxysilane (APTES), pyrene (Py), coumarin 153 (C153) and fluorescein isothiocyanate (FITC) were all purchased from Sigma-Aldrich and used as received. All solvents were obtained from Sigma-Aldrich or Fischer Scientific and used without further purification. Water was purified using a Millipore SimPak® 2 water purification system and filtered three times through a 0.2 µm nylon filter before use. The dialyses were performed using snake-skin pleated dialysis tubing from Thermoscientific with a M_w cut-off of 3,500 Da.

Synthesis of the d-UPTES Precursor

The organic-inorganic hybrid framework d-UPTES was synthesized in quantitative yield, by reacting the terminal amine functionalities of Jeffamine ED-600 with the isocyanate group of an alkoxysilane precursor, as reported in detail elsewhere.[34,38] In brief, ICPTES (0.91 mL, 3.7 mmol) was mixed with Jeffamine ED-600 (1 mL, 1.8 mmol) in THF (5 mL) and reacted for 24 h at room temperature. Reaction completion was confirmed by recording Fourier transform infrared (FTIR)

spectra over the 4000-650 cm^{-1} range (1 cm^{-1} resolution). The appearance of broad N-H (~3400-3600 cm^{-1}) and C=O (1610-1770 cm^{-1}) stretching signals and the concomitant disappearance of the isocyanate N=C=O stretch at 2265 cm^{-1} are indicative of the presence of urea linkages and thus, formation of the hybrid di-ureasil precursor d-UPTES (see **Figure S1**, ESI).[38]

Synthesis of ureasil core-shell nanocomposite particles

In a typical synthesis, an aliquot of the as-prepared d-UPTES stock solution (54.8 µL, 0.56 M) was added to a sample tube containing THF (671.2 µL) to obtain a concentration of 20,000 ppm. In a second sample tube (soda glass, diameter 25 mm and length 75 mm), ammonium hydroxide was added to triple-filtered Millipore water to obtain 3 mL of basic water (10 mM NH_4OH unless otherwise stated). The diluted d-UPTES solution in THF was then injected vigorously into the basic water solution using a disposable syringe (2 mL) fitted with a BRAUN Sterican needle (diameter 0.45 mm and length 25 mm) to obtain the particle cores. To afford the growth of a sufficiently thick silica shell around the core, TEOS was added in a single or stepwise manner at different stages of the synthesis. In Method A, TEOS (24 µL, 50%$_{v/v}$ in THF) was mixed with d-UPTES in THF and injected in a single step into the NH_4OH solution (co-condensation). In Method B, the addition of TEOS (120 µL, 5%$_{v/v}$ in THF) was performed drop-by-drop in one single step after the formation of d-UPTES cores. Finally, in Method C, the TEOS addition was also performed after the injection of d-UPTES in the basic aqueous solution, but contrary to Method B, this was done via multiple additions (n = 2) of 60 µL of a solution of TEOS (5%$_{v/v}$ in THF) over a period of 2 hours. At the end of each method, THF was completely removed from the particle dispersion using a rotary evaporator at room temperature. Additional details on the specific conditions used in Methods A-C can be found in the ESI (Table S1).

Synthesis of fluorophore-doped core-shell composite particles (Py@CSNPs and C153@CSNPs)

Stock solutions of pyrene and Coumarin 153 (3×10^{-3} mol L^{-1}) were prepared in THF. The encapsulation of the fluorescent dyes within the core of the NPs was achieved by mixing the required volume of dye stock solution (24.6 µL for Py, 36.0 µL for C153) to the d-UPTES solution prior to the injection into basic water solution. The volume of THF used to dilute the d-UPTES stock solution was adjusted to keep the overall d-UPTES concentration consistent with that used for undoped NPs. The remaining steps for the particle synthesis are the same as described above. For C153@CSNPs, the resultant particle suspension (~3 mL ureasil CSNPs) was dialyzed against a 10 mM solution of NH_4OH in water to maintain the charge on the NP surface. Dialysis ensures the absence of free fluorophore in solution as the encapsulation within the core is not quantitative.

Synthesis of fluorophore-grafted core-shell nanocomposite particles (FITC@CSNs)

FITC (0.0135 mmol) was pre-reacted with APTES (0.405 mmol) in 1 mL of EtOH at RT, in the dark and under an N_2 atmosphere for 24 hours. Although the reaction occurs in a 1:1 molar ratio, an excess of APTES to FITC (30:1 molar ratio) was used to ensure that the silica precursor is grafted to all dye molecules (FITC-PTES). The reaction mixture was centrifuged (7 min, 10,000 rpm) and the supernatant collected. The synthesis of the NPs was performed using the same quantities and conditions described in Method C. During the second addition of TEOS, an aliquot of the supernatant containing FITC-PTES (either 3, 6 or 15 µL) was co-added with the TEOS into the reaction mixture. The same aliquot was subtracted by the volume of TEOS added (e.g. 3 µL of supernatant + 57 µL of TEOS) in order to keep the total volume added constant. Residual THF and EtOH were then removed with a rotary evaporator (10 min, RT). Detailed information on the different sample conditions can be found in Table S2, ESI.

Characterization

FTIR spectroscopy. Confirmation of the formation of the d-UPTES intermediate was performed using a Perkin-Elmer Spectrum 100 FTIR spectrometer equipped with an attenuated total reflection (ATR) accessory.

Dynamic Light Scattering (DLS). The hydrodynamic diameter (D_h) of the NPs was recorded in solution at 293 K using a Zetasizer Nano series nano-ZS instrument (Malvern Instruments, U.K.). The instrument is equipped with a He-Ne laser (λ_{ex} = 633 nm) and uses backscatter detection at a scattering angle of 173°. Typically, 100 µL of NP solution was added to 900 µL of triple-filtered water and measured in a disposable acrylic cuvette (Sarstedt, 10 mm pathlength).

A temperature equilibration time of 2 minutes was set to run prior to each measurement, which consisted of 3 runs of at least 15 scans each. ζ-potential measurements were performed on the same instrument, with the use of disposable capillary cells from Malvern Instruments (DTS1070).

Atomic Force Microscopy (AFM). Samples were prepared by drop-casting 40 µL of NP dispersion, diluted 50 times in tripled-filtered water, onto a Mica sheet before air-drying overnight. Measurements were performed using an Asylum Research MFP-3D™ Atomic Force Microscope mounted on an anti-vibration plinth, in the tapping mode at room temperature under ambient conditions. The silicon cantilevers used were 125 µm in length and had a resonance frequency of approximately 150 kHz. All raw AFM images were visualized and analyzed using the Gwyddion 2.31 software.

UV-Vis absorption and photoluminescence (PL) spectroscopy. Unless otherwise stated, all measurements were performed in aqueous solution at room temperature using 1 cm path length quartz cuvettes from Hellma. UV-visible absorption spectra were measured either on a Shimadzu UV2401 PC UV-Vis scanning spectrometer or on a Perkin Elmer Lambda 1050 UV/vis/NIR spectrophotometer. Baseline correction was applied for all spectra. Steady-state PL measurements were performed using a Horiba Scientific Fluoromax–4 spectrophotometer. All emission and excitation spectra were corrected for the wavelength response of the system using correction factors supplied by the manufacturer. For these measurements, NP dispersions were diluted by adding 200 µL of NP stock to 1.8 mL of triple-filtered water.

Time-resolved PL spectroscopy. Fluorescence lifetime measurements were performed using a Horiba Fluorolog FL 3-22 spectrometer equipped with a FluoroHub v2.0 single photon controller using the time-correlated single photon counting method. Samples were excited at 458 nm with a pulsed nanosecond light-emitting diode (NanoLED®). The time distribution of the lamp pulse (<1.3 ns) was recorded prior to lifetime measurements in a separate experiment using a scattering solution (Ludox). Reconvolution and data-fitting were performed as an individual fit to each decay using DAS6 software (Horiba).The quality of fits were judged from the reduced chi-square statistic, χ2, and the randomness of residuals.

Live/Dead Cell Assay. HEK293 cells (Human embryonic kidney cells) were grown in Advanced DMEM (Dulbecco's Modified Eagle Medium, GIBCO/Life Technologies), supplemented with 10% Fetal Bovine Serum (FBS, Heat-Inactivated, Sigma-Aldrich), 2 mM GlutaMAX (GIBCO/Life Technologies), 0.5% Penicillin-Streptomycin (GIBCO/Life Technologies), 50 µg/ml Gentamicin (GIBCO/Life Technologies) and placed into a humidified incubator in 5% CO2. Cells were seeded at 300,000 cells/cm2 and allowed to adhere for two hours. Nanoparticles were prepared at a stock concentration of 7.5 mg/ml and diluted in the cell-growth medium before addition to cells in the concentration range of 0.001-1mg/ml. A Live/Dead Assay (Life Technologies) was performed 24 hours after seeding, using calcein AM to stain live cells and ethidium homodimer-1 (EtHD1) to stain dead cells. The samples were imaged using a confocal microscope (AxioObserver Z1, Carl Zeiss MicroImaging GmbH) using the following excitation/emission wavelengths: calcein AM (494 nm /514 nm) and EtHD1 (350 nm /617 nm).

Results and Discussion

Design Strategy

Our synthetic pathway to obtain ureasil CSNPs combines two routes: nanoprecipitation[18] and the Stöber method.[25] The precursor d-UPTES (**Figure 1a**) was synthesized by reacting Jeffamine ED-600 and ICPTES in THF, which is a good solvent for the reagents and d-UPTES. Then, an aliquot of d-UPTES was sprayed onto the surface of a solution of a bad solvent (basic water, pH 10.8) to yield the NP core (**Figure 1b**, step [1]). The transfer d-UPTES from a good to a poor solvent is expected to drive hydrophobic aggregation of the precursor into nuclei, from which the ureasil CSNPs can grow.[24] Considering the chemical structure of d-UPTES, it is expected that the nuclei of the ureasil CSNPs would be formed by the poly(ether) chains, with the ethoxysilane extremities exposed at the surface. Ammonium hydroxide present in solution triggers the hydrolysis-condensation sol-gel reaction of the surface siloxane groups (**Figure 1b**, step [2]), resulting in the formation of a thin silica shell – this is reminiscent of the standard ureasil structure. TEOS was then added to control the thickness of the silica shell and to improve the stability in solution (**Figure 1b**, step [3]).[3] The additional TEOS is expected to co-condense with the exposed ethoxysilane groups and reinforce the silica shell. The final particles are expected to consist of an organic polyether core, an intermediary ureasil organic-inorganic boundary, and an inorganic silica shell.

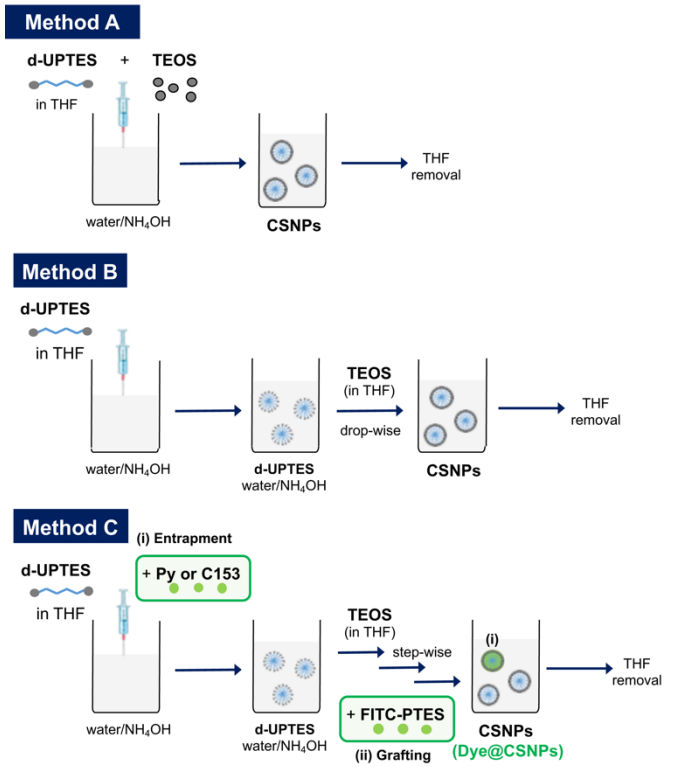

Figure 2. Evolution of the synthetic process to prepare stable ureasil core-shell nanoparticles. Method C additionally illustrates the approach used to either (i) physically entrap pyrene (Py) or coumarin 153 (C153) or (ii) graft fluorescein (FITC-PTES) to the nanoparticles.

Optimization of Synthetic Route

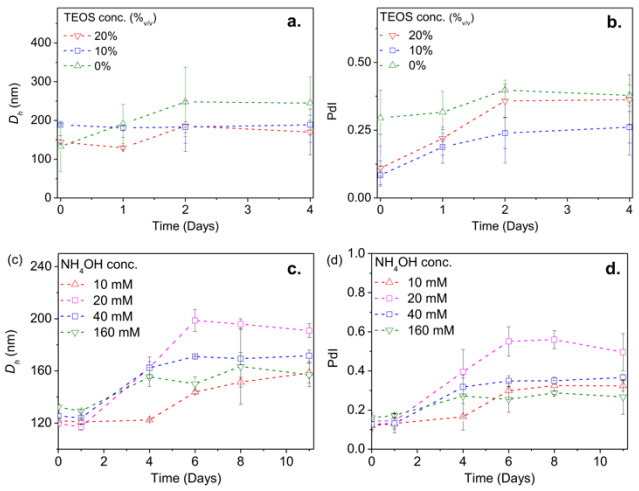

Figure 3. Time-dependent stability studies of ureasil CSNPs prepared using Method B using different TEOS and base concentrations. Evolution of the hydrodynamic diameter, D_h (a, c) polydispersity, PdI (b, d) as a function of time. The dashed lines serve only to guide the eye. The data points are the average values obtained for three

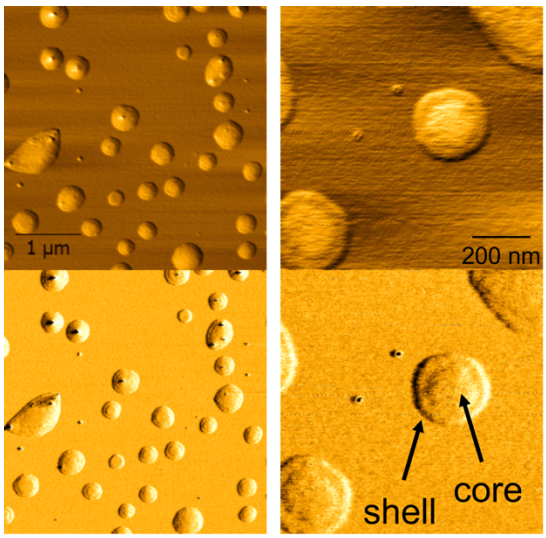

Figure 4. Tapping-mode AFM images of ureasil CSNPs made using Method B. Top panel – height-contrast images; Lower panel – phase contrast images. The core-shell structure of the nanoparticles is also indicated.

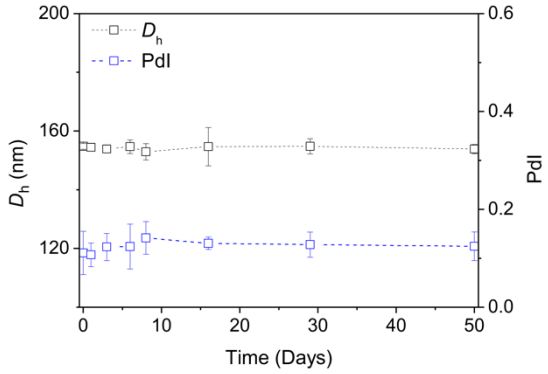

Figure 5. Time-dependent stability of the hydrodynamic diameter (D_h) and polydispersity (PdI) of ureasil CSNPs prepared using Method C with a TEOS addition rate of 60 µL/60 mins in a 10 mM NH_4OH solution.

Despite the simple design strategy, several synthetic parameters and steps had to be optimised to yield stable ureasil CSNPs. The evolution of the synthetic method is summarised in **Figure 2**. All methods involved the removal of residual THF as the final step to reduce the possibility of Ostwald ripening.[39] The initial and most straightforward approach involved pre-mixing d-UPTES in THF with TEOS, followed by rapid injection of the mixture into basic water (**Figure 2**a, Method A). The concentration of d-UPTES (20,000 ppm), volume of water (3.0 mL), base (12 µL, 0.06 mmol) and TEOS (24.0 µL, 0.05 mmol, 50% v/v in THF) were initially selected arbitrarily and kept constant. As shown in **Figure S2** (ESI), ureasil CSNPs obtained using Method A had an average hydrodynamic diameter (D_h) ranging between 122-164 nm and a polydispersity (PdI) of 0.11. However, despite these promising results, it was noticed that after 3 days, the NP dispersions turned opaque, indicating the formation of larger particles or even aggregates. This was confirmed by monitoring the time-dependent stability (over 48 hours) of different samples prepared using Method A, which showed a progressive increase in both PdI and D_h with time after synthesis (**Figure S3**, ESI). As the ureasil CSNPs are expected to be stabilized by negatively-charged silanol units on the particle surface,[23] the observed instability suggested that co-injection of d-UPTES and TEOS does not result efficient self-compartmentalization of the hydrophobic core and charged silica shell. This might be due to the partially polar nature of the Jeffamine chains.

To better control shell formation, the procedure was modified to separate the nanoprecipitation and Stöber steps (Method B, **Figure 2**b), with d-UPTES injected first to yield the core and the TEOS subsequently added dropwise to reinforce the shell. Ureasil CSNPs were prepared using different amounts of TEOS in THF (from 0 to 20%$_{v/v}$), while the overall volume added (120 µL) was kept constant. The PdI and D_h were monitored over the course of 4 days (**Figure 3**a and b). The largest sizes and PdI were measured for ureasil CSNPs prepared without TEOS (0%), with both D_h and PdI increasing during the first two days after preparation, from 133 nm to 245 nm and from 0.25 to 0.38, respectively, and then stabilizing at D_h > 200 nm. This confirmed our hypothesis that the silica shell provided only by the d-UPTES is not sufficiently dense to stabilize the NPs. Conversely, while a very high TEOS concentration (20%$_{v/v}$) afforded good particle sizes (129-170 nm), but led to higher values of PdI, reaching a maximum of 0.36. This is believed to be due to the formation of a separate population of pure SiO_2 NPs (**Figure S4,** ESI). The ureasil CSNPs with the best time-dependent size/distribution properties were obtained for a TEOS concentration of 10 %$_{v/v}$, with D_h and PdI of 189 nm and 0.26, respectively, after 4 days.

To improve colloidal stability, the effect of the concentration of base catalyst (10-160 mM) was then investigated over 10 days. Despite promising D_h values (below

200 nm at any time and/or base concentration), the PdIs were strongly influenced by the base concentration. Based on the results summarized in **Figure 3**c,d, the best size/PdI combination was obtained for samples prepared using the lowest and the highest ammonium hydroxide concentrations (10 mM and 160 mM, respectively), which both yield ureasil CSNPs with an average diameter of ~160 nm and a PdI of ~0.3 after 10 days. Previous studies showed that an increase in base concentration is usually correlated to an increase in the rate the sol-gel reaction, due to an increase in the concentration of the intermediate semi-hydrolyzed products of the reaction.[40] When the system reaches the supersaturation limit, the consumption rate of any intermediate units through condensation reactions will also be very fast, which can lead to a decrease in the nucleation period.[41] This results in lower numbers of critical nuclei in solution and larger particle sizes compared to those observed in the same systems with a lower catalyst concentration.[41] Based on this knowledge and the experimental data obtained, the base concentration was fixed at 10 mM for subsequent iterations of the synthetic procedure. The core-shell architecture of the obtained particles was confirmed by AFM (**Figure 4**). We note that the particle diameter obtained by AFM (~240 nm) is unusually larger than that measured by DLS (~200 nm). This is mostly likely due to the need to dilute the stock sample (1:50 *v/v* in water) to obtain images of individual particles by AFM, leading to a decrease of the pH and destabilization of the NPs.[42]

Although sequential addition of the reagents led to significant improvement in the particle size and structure, the colloidal stability was still insufficient. The poor time-dependent stability was believed to most likely be due to poor shell coverage. To overcome this problem, a "semi-batch" process was adopted, in which the required volume of TEOS was added over a series of steps, allowing time between each addition (**Figure 2**c, Method C). This approach facilitated progressive formation of the silica shell, allowing a better coverage and improved size control of the final ureasil CSNPs. A series of samples was prepared where the TEOS solution (5%$_{v/v}$, in THF) was added as separate aliquots over 2 hours, up to a maximum volume of 120 µL. The effect of the aliquot volume was investigated and the concentration of NH_4OH was also monitored for different TEOS addition rates. The size and PdI of ureasil CSNPs measured immediately after preparation using Method C are very promising, with an average D_h of ~130-155 nm and PdIs below 0.15 (**Figure 5** and **Figure S5**, ESI). The most stable samples were obtained using two 60 µL aliquots of TEOS added at 60 minute intervals, which retained a D_h of 152 (± 2) nm and PDI 0.12 (± 0.03) up to 50 days after synthesis, without applying any particular storage conditions. The corresponding ζ-potential was also measured and found to be -51.3 ± 3.3 mV, indicating good colloidal stability.[43] Therefore, Method C and these specific stepwise reaction conditions were used as the optimized synthetic procedure for the preparation of stable ureasil CSNPs.

Preparation of Fluorescent Core-Shell Nanocomposite Particles

The preparation of fluorescent ureasil CSNPs was investigated to probe the internal environment. Two synthetic routes were followed: (i) physical entrapment of a fluorescent dye within the ureasil CSNP, and (ii) covalent grafting of a fluorescent dye within the silica shell. Both routes were designed to minimize modifications to the optimized synthesis, in order to preserve not only the NP structure, but also their stability.

Considering the physical approach first, two polarity-sensitive dyes, namely pyrene (Py) and Coumarin 153 (C153), were mixed with d-UPTES in THF, prior to injection into the basic water solution, and ureasil CSNPs were synthesized using Method C (**Figure 2**). Given the hydrophobic nature of both Py and C153, it is expected that the dyes will preferentially localize within the d-UPTES core of the NPs.

Py-doped core-shell NPs (Py@CSNPs) showed a D_h of 149 ± 2 nm and PdI of 0.08 ± 0.01. The polarity-dependent spectroscopic behavior of pyrene can be extrapolated from: (i) the ratio between the emission intensities of the third and the first vibronic peaks in the photoluminescence (PL) spectrum (I_3/I_1 ratio) and (ii) the presence of a broad band centered at ~465 nm, indicative of the excimer formation and usually present when the dye aggregates (*i.e.* in confined environments).[44,45] The PL spectrum of Py@CSNPs is characterized by the typical features of monomeric pyrene (**Figure 6**a), with a vibronically-structured emission band between 350 and 450 nm. In addition, the broad excimeric emission band is also observed, centred at ~470 nm. To simulate the water/d-UPTES environment, the PL properties of Py were water/ethanol mixtures at different (v/v) ratios and compared to those obtained for Py@CSNPs (**Figure S6**, ESI), suggesting that the internal particle polarity is intermediate to that of pure EtOH or pure water.

Interestingly, the intensity of the excimer emission first increases from t = 2 h to 6 h, and then decreases progressively with time. Across the same time period, the corresponding I_3/I_1 ratio decreases from 0.68 to 0.64 (**Figure 6b**), which is higher than that of pure pyrene in water (0.59, **Figure S6**, ESI), and then continues to decrease to 0.59 after 48 hours. A small increase in both the size (149 to 177 nm) and PdI (0.08 to 0.26) was also observed over this time period. These results suggest that the fluorophore is initially incorporated inside the NPs (as indicated by the high initial I_3/I_1 ratio), but appears to slowly leach out with time. Although tempting to assume that the excimer emission observed for Py@CSNPs is indicative of the confinement of pyrene units in the core, dye aggregation is clearly observed in water as well at this concentration (**Figure 6a**).

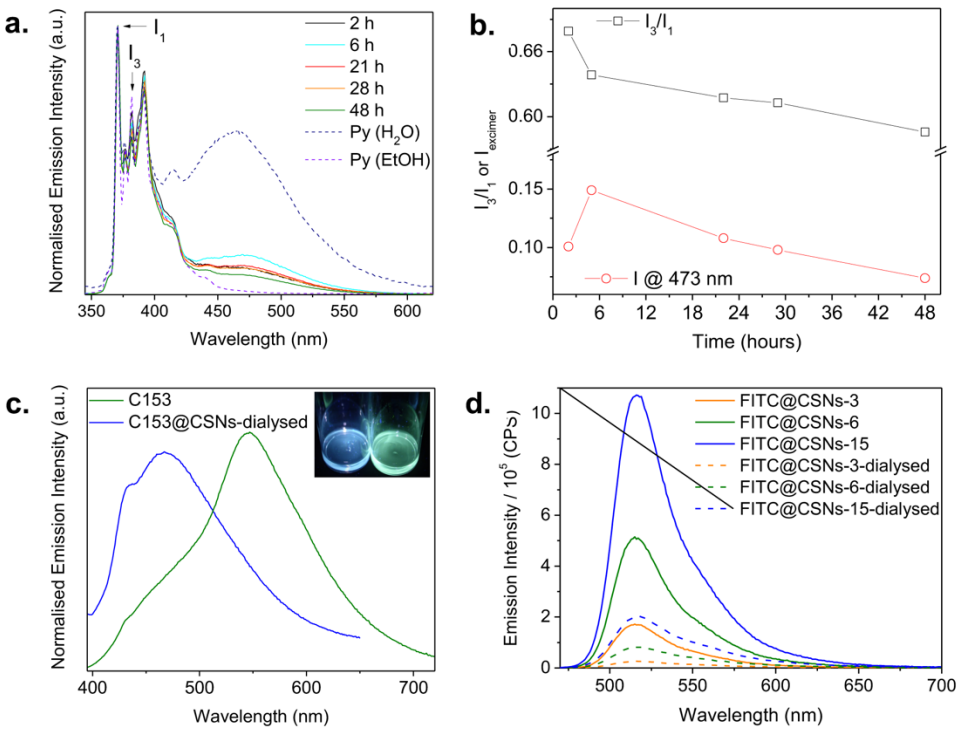

Figure 6. Fluorescence properties of ureasil core-shell nanoparticles containing physically-entrapped or covalently-bound fluorescent dyes. (a) Time-dependent evolution of the normalized emission spectrum of Py@CSNPs (solid coloured lines) and Py in water and ethanol (2.5×10^{-5} mol L^{-1}, dashed lines). λ_{ex} =335 nm. The vibronic peaks, I_1 and I_3, are also indicated. (b) I_3/I_1 ratio for Py@CSNPs over time (open black squares) and normalized intensity of the emission maximum of the excimer emission (open red circles). The lines serve only to guide the eye. (c) Normalized emission spectra of C153 (3.6×10^{-5} mol L^{-1} in water, green solid line) and of C153@CSNPs after dialysis (blue dashed line). λ_{ex} = 420 nm. The inset shows a photograph of the corresponding samples under UV irradiation (λ_{ex} = 366 nm). (d) Emission spectra of FITC@CSNPs before (solid lines) and after (dashed lines) dialysis (24 hours). λ_{ex} = 465 nm.

C153@CSNPs prepared in the same way had a D_h of 117 ± 2 nm, with a PdI of 0.14 ± 0.03. The emission spectrum of coumarin 153 is known to undergo a blue-shift when the polarity of its environment is decreased.[46,47] The PL spectrum of C153 in water exhibits a broad band between 430 and 680 nm, with a maximum at ~549 nm (**Figure 6c**) The PL spectrum of as-synthesized C153@CSNPs is comparable, but the emission maximum is slightly blue-shifted ($\Delta\lambda$ = -2 nm, **Figure S7**, ESI). The corresponding excitation spectra are also similar for both samples, exhibiting a broad band from 330 to 500 nm (λ_{max} = 411 nm, **Figure S7**, ESI). More significant differences are observed in the UV/Vis absorption spectra, whose maximum is blue-shifted for the C153@CSNPs compared to C153 in water (418 nm *vs* 429 nm, respectively, **Figure S7**, ESI). This suggests that ground-state interactions, namely aggregation, dominate for C153 in water.[48] The results suggest that the spectroscopic properties of both samples are dominated by that of the free dye in water, which may be swamping the emission from C153@CSNs. To test this hypothesis, the C153@CSNP dispersion was dialyzed for 24 hours against a NH_4OH/water solution (pH 9) to remove excess C153 and the emission spectrum was re-measured (**Figure 6c**). A dramatic blue-shift was observed in the PL spectrum ($\Delta\lambda_{max}$ = -79 nm), with the emission colour changing from green to blue. This behaviour is indicative of the dye residing in a less polar environment,[48] proving successful incorporation of C153 within the NP core.

For the grafting approach, fluorescein isothiocyanate (FITC) was selected as the fluorophore since it can readily be reacted with the amine moiety of a siloxane precursor such as 3-aminopropyltriethoxysilane (APTES), and the resulting product (FITC-PTES) can be co-condensed to the silica shell of the CSNPs.[49,50] FITC-PTES was introduced by co-addition with the TEOS during the second step of the reaction (Method C), with an equivalent aliquot of TEOS subtracted from the final volume to maintain the thickness of the silica shell. Three different concentrations of FITC-PTES were tested and reference samples containing only APTES were also prepared to investigate whether the potential addition of amine groups to the NPs surface could affect the colloidal stability. The composition of the prepared samples is reported in **Table S2,** ESI.

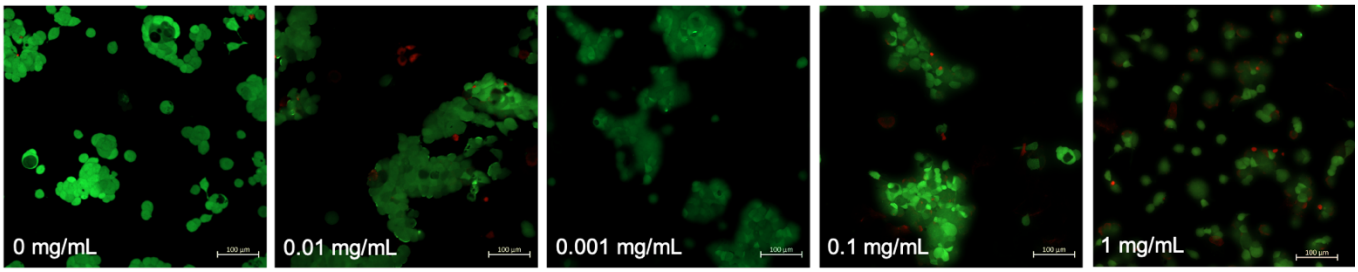

Figure 7. Ureasil CSNPs nanoparticles do not display cytotoxicity**.** HEK 293 cells were exposed to ureasil CSNPS at various concentrations from 0.001-1 mg/ml for 24 hours. A live/dead assay (Calcien AM/Ethidium homodimer) was performed to assess cytotoxicity. Scale bar is 100 µm.

The stability of the CSNPs was monitored, and the diameters and PdI ranged between 100-210 nm and 0.01-0.21, respectively, for both the APTES@CSNP and FITC@CSNP series after 13 days (**Figure S8**, ESI). The emission spectra of FITC@CSN samples were measured before and after dialysis to determine if the dye was effectively covalently grafted into the silica shell (**Figure 7d**). The PL spectra of FITC@CSNs before and after dialysis exhibit the typical optical features of fluorescein,[50] however, after dialysis a significant decrease in the emission intensity is observed (80-85% of the initial intensity), indicating the presence of an excess of un-bound dye which may have resulted from poor yields in the preparation of the FITC-PTES.

To ensure that the observed emission properties were due to FITC moieties grafted onto the NPs and not only un-bound dye in solution, fluorescence lifetime measurements were performed. To compare differences between systems containing fluorescein, either bound or unbound to APTES, a sample consisting of fluorescein sodium salt (FNa) and APTES was prepared in the same molar ratios and conditions used to form the FITC-PTES precursor and the resultant FNa-APTES solution was added during the NP synthesis (sample FNa-APTES@CSNP), using the same concentration as FITC@CSNP-3. Although no reaction is expected to occur between the two species, the APTES is expected to graft onto the surface of the NPs, thus influencing the system stability and/or the FNa distribution to some extent. The emission decay curve, fits and residuals are shown in **Figure S9** (ESI) while the results of the lifetime fittings are presented in **Table S3** (ESI).

As expected, the decay curve of FNa-APTES is comparable to that of pure fluorescein in ethanol and is characterized by a single emission lifetime, τ_1 = 4.1 ns.[50] The emission decays of FNa-APTES@CSNPs are also monoexponential (τ_1 ~4.0 ns), and are unchanged even when measuring the solution after the first and second dialysis (**Figure S9**, ESI). It worth noting that the solution progressively loses most of its green emission during the dialysis processes, as expected from the aforementioned experiments. The FITC-PTES decay curve is also monoexponential, with a similar lifetime (τ_1 = 3.8 ns) to that of FNa-APTES (**Figure S9**, ESI). Interestingly, upon incorporation into the NPs, the decay curve can only be modeled using a biexponential fit (τ_1 ~3.9 ns and τ_2 ~ 2.0 ns), which is in good agreement with that observed in the literature for fluorescein in different environments.[50] A slight redistribution of the fractional contribution (f_i) values is observed after the first dialysis, with an increase in f_1 (from 0.44 to 0.67) and a concomitant decrease in f_2 (from 0.56 to 0.33). These values remained constant upon the second dialysis and could indicate re-distribution of the FITC molecules onto the NP surface.

Although these data cannot unravel the exact location of the FITC units in the NPs, they can give us further insight into their organization in solution and onto the NPs. It is reasonable to assume that a portion of the FITC molecules is grafted onto the inner silica shell of the NPs, occupying the vacant holes in the ureasil cores left uncovered by the first TEOS addition. A second population of FITC molecules could actually be located on the surface of the NPs, with the APTES extremity covalently grafted onto the outer silica shell. It is also possible that some of the fluorescein molecules are stacked on the surface of the NPs, interacting with the covalently bound FITC-PTES units. It is also important to note that during the dialysis the volume of sample inside the dialysis bag increased progressively with time, and that the resulting dilution of the NPs solution could have led to the re-dispersion of the dye into the solution by inhibiting the potential stacking interactions discussed above. Overall these data showed that FITC-PTES exists in two different environments within the ureasil CSNP dispersion.

Cell toxicity studies

A Live/Dead Assay was performed to make a preliminary assessment of the cytotoxicity of the ureasil CSNPs. The assay uses two stains: (1) calcein AM, which can enter live cells, where it is enzymatically converted to the intensely fluorescent calcein dye in the cytosol of live cells, and (2) ethidium homodimer, which can only enter into dead cells and becomes fluorescent upon binding to nucleic acids inside the cells. The results shown in Figure 7 show that the silica nanoparticles did not affect HEK 293 cell viability, with only negligible numbers of dead cells seen at the highest concentration of nanoparticle. Further studies will be required to assess the mechanism for nanoparticle uptake, and to understand how this is affected by the surface chemistry, size and porosity of the nanoparticles, which are factors known to affect the cytotoxicity of silica-based nanoparticles.[12]

Conclusions

A one-pot liquid phase method to synthesise ureasil CSNPS has been demonstrated. The optimised synthetic conditions

were found to be: (i) d-UPTES concentration of 20,000 ppm (ii) base concentration equal to 10 mM NH_4OH, (iii) TEOS concentration of 5%v/v in THF and (iv) rate of addition of TEOS equal to 60 µL/ 60 minutes. The ureasil CSNPs obtained following this method present sizes of ~150 nm and PdI < 0.2 and the aqueous dispersions are stable for over 50 days. As hypothesised, formation of the core-shell architecture is facilitated by the terminal triethoxysilane groups on d-UPTES, which act as a suitable template for the nucleation and growth of the silica shell, as indicated by AFM imaging.

The encapsulation of fluorescent organic dyes was explored using both physical entrapment and grafting approaches to investigate the internal environment and retention within ureasil CSNPs. For Py-loaded NPs, the dye tended to leach out of the aggregates roughly two days after encapsulation, which is attributed to the inherent polarity of the Jeffamine chains which constitute the core material. In contrast, C153 remained encapsulated within the ureasil CSNPs even after dialysis. Covalent-grafting of FTIC to the silica shell was also demonstrated, with PL lifetime measurements suggesting the presence of two distinct environments, assigned to the inner and outer shell regions.

The power of the approach presented here lies both in its simplicity and versatility. A huge variety of Jeffamine™ precursors are readily-available[51], which facilitates tuning of the mechanical and chemical properties of the core, *e.g*. solvent swelling, localised polar/apolar environments. Physical and grafting methods enable localisation of fluorescent dyes (or other responsive species) to distinct regions of the core-shell structures. Given that preliminary studies using a live/dead cell assay indicate that ureasil CSNPs do not display cytotoxicity at the concentrations tested, this paves the way to potential applications in cell imaging and sensing. Future efforts will be focussed on further investigating the ureasil CSNP system to investigate the effect of the precursor polymer chain length and branching on the particle permeability and structure. Known grafting chemistry methods will also be exploited to locate donor-acceptor fluorophore pairs within specific regions of the core-shell structure to design a fluorescence resonance energy transfer (FRET) based sensing scheme aimed at biomarker detection.

Conflicts of interest

There are no conflicts to declare.

Acknowledgements

This work was supported in part by the Science Foundation Ireland under Grant No. 12/IP/1608 and by an Isaac Newton Trust/University of Cambridge Early Career Support Scheme grant.

References

1 L. C. Hu and K. J. Shea, *Chem. Soc. Rev.*, 2011, **40**, 688–695.
2 A. E. Danks, S. R. Hall and Z. Schnepp, *Mater. Horizons*, 2016, **3**, 91–112.
3 R. Ghosh Chaudhuri and S. Paria, *Chem. Rev.*, 2012, 112, 2373–2433.
4 T. Ribeiro, C. Baleizão and J. P. S. Farinha, *J. Phys. Chem. C*, 2009, **113**, 18082–18090.
5 R. Zhang, C. Wu, L. Tong, B. Tang and Q.-H. Xu, *Langmuir*, 2009, **25**, 10153–10158.
6 J. M. Behrendt, A. B. Foster, M. C. McCairn, H. Willcock, R. K. O'Reilly and M. L. Turner, *J. Mater. Chem. C*, 2013, **1**, 3297–3304.
7 Y. Yang, X. Wang, G. Liao, X. Liu, Q. Chen, H. Li, L. Lu, P. Zhao and Z. Yu, *J. Colloid Interface Sci.*, 2018, **509**, 515–521.
8 T. C. Gardinier, F. F. E. Kohle, J. S. Peerless, K. Ma, M. Z. Turker, J. A. Hinckley, Y. G. Yingling and U. Wiesner, *ACS Nano*, 2019, **13**, 1795–1804.
9 S. P. Meaney, B. Follink and R. F. Tabor, *ACS Appl. Mater. Interfaces*, 2018, **10**, 43068–43079.
10 S. Masse, G. Laurent, F. Chuburu, C. Cadiou, I. Déchamps and T. Coradin, *Langmuir*, 2008, **24**, 4026–4031.
11 Q. Huo, J. Liu, L. Q. Wang, Y. Jiang, T. N. Lambert and E. Fang, *J. Am. Chem. Soc.*, 2006, **128**, 6447–6453.
12 L. Tang and J. Cheng, *Nano Today*, 2013, **8**, 290–312.
13 W. Ma, S. Sha, P. Chen, M. Yu, J. Chen, C. Huang, B. Yu, Y. Liu, L. Liu and Z. Yu, *Adv. Healthc. Mater.*, 2020, **9**, 1901100.
14 M. Destribats, S. Gineste, E. Laurichesse, H. Tanner, F. Leal-Calderon, V. Héroguez and V. Schmitt, *Langmuir*, 2014, **30**, 9313–9326.
15 N. J. Fernandes, J. Akbarzadeh, H. Peterlik and E. P. Giannelis, *ACS Nano*, 2013, **7**, 1265–1271.
16 X.-J. Cai, H.-M. Yuan, A. Blencowe, G. G. Qiao, J. Genzer and R. J. Spontak, *ACS Nano*, 2015, **9**, 7940–7949.
17 X. Hu and X. Gao, *ACS Nano*, 2010, **4**, 6080–6086.
18 Z. Tian, J. Yu, C. Wu, C. Szymanski and J. McNeill, *Nanoscale*, 2010, **2**, 1999–2011.
19 Y. Chen and Z. Guan, *Polym. Chem.*, 2013, **4**, 4885–4889.
20 X. Zhou, W. Li, L. Zhu, H. Ye and H. Liu, *RSC Adv.*, 2019, **9**, 1782–1791.
21 T. Engel and G. Kickelbick, *Polym. Int.*, 2014, **63**, 915–923.
22 Q. Shi, Z. An, C. K. Tsung, H. Liang, N. Zheng, C. J. Hawker and G. D. Stucky, *Adv. Mater.*, 2007, **19**, 4539–4543.
23 H. E. Bergna and W. O. Roberts, *Colloidal Silica: Fundamentals and Applications*, CRC Press, Boca Raton, vol. 131., 2006.
24 R. Liu and R. D. Priestley, *J. Mater. Chem. A*, 2016, **4**, 6680–6692.
25 W. Stöber, A. Fink and E. J. Bohn, *J. Colloid Interface Sci.*, 1968, **26**, 62–69.
26 A. Kaniyoor, B. Mckenna, S. Comby and R. C. Evans, *Adv. Opt. Mater.*, 2016, **4**, 444–456.
27 G. Lyu, J. Kendall, I. Meazzini, E. Preis, S. Bayseç, U. Scherf, S. Clément and R. C. Evans, *ACS Appl. Polym. Mater.*, 2019, **1**, 3039−3047.
28 A. R. Frias, E. Pecoraro, S. F. H. Correia, L. M. G. Minas, A. R. Bastos, S. García-Revilla, R. Balda, S. J. L. Ribeiro, P. S.

André, L. D. Carlos and R. A. S. Ferreira, *J. Mater. Chem. A*, 2018, **6**, 8712–8723.
29 S. F. H. Correia, A. R. Frias, L. Fu, R. Rondão, E. Pecoraro, S. J. L. Ribeiro, P. S. André, R. A. S. Ferreira and L. D. Carlos, *Adv. Sustain. Syst.*, 2018, **2**, 1800002.
30 A. Bastos, B. McKenna, M. Lima, P. S. André, L. D. Carlos, R. C. Evans and R. A. S. Ferreira, *ACS Omega*, 2018, **3**, 13772–13781.
31 P. Barbosa, L. Rodrigues, M. Silva, M. Smith, A. Gonçalves and E. Fortunato, *J. Mater. Chem.*, 2010, **20**, 723–730.
32 I. Meazzini, N. Willis-Fox, C. Blayo, J. Arlt, S. Clément and R. C. Evans, *J. Mater. Chem. C*, 2016, **4**, 4049–4059.
33 I. Meazzini, J. M. Behrendt, M. L. Turner and R. C. Evans, *Macromolecules*, 2017, **50**, 4235–4243.
34 N. Willis-Fox, A. T. Marques, J. Arlt, U. Scherf, L. D. Carlos, H. D. Burrows and R. C. Evans, *Chem. Sci.*, 2015, **6**, 7227–7237.
35 R. Rondão, A. R. Frias, S. F. H. Correia, L. Fu, V. De Zea Bermudez, P. S. André, R. A. S. Ferreira and L. D. Carlos, *ACS Appl. Mater. Interfaces*, 2017, **9**, 12540–12546.
36 I. Meazzini, C. Blayo, J. Arlt, A. T. Marques, U. Scherf, H. D. Burrows and R. C. Evans, *Mater. Chem. Front.*, 2017, **1**, 2271–2282.
37 R. A. S. Ferreira, P. S. André and L. D. Carlos, *Opt. Mater. (Amst).*, 2010, **32**, 1397–1409.
38 V. De Zea Bermudez, L. D. Carlos and L. Alcácer, *Chem. Mater.*, 1999, **11**, 569–580.
39 T. K. N. Hoang, L. Deriemaeker, V. B. La and R. Finsy, *Langmuir*, 2004, **20**, 8966–8969.
40 G. H. Bogush and C. F. Zukoski IV, *J. Colloid Interface Sci.*, 1991, **142**, 1–18.
41 S.-L. Chen, P. Dong, G.-H. Yang and J.-J. Yang, *Ind. Eng. Chem. Res.*, 1996, **35**, 4487–4493.
42 R. Brydson, A. Brown, C. Hodges, P. Abellan and N. Hondow, *J. Microsc.*, 2015, **260**, 238–247.
43 J. D. Clogston and A. K. Patri, *Methods Mol. Biol.*, 2011, **697**, 63–70.
44 K. Kalyanasundaram and J. K. Thomas, *J. Am. Chem. Soc.*, 1977, **99**, 2039–2044.
45 V. R. Kaufman and D. Avnir, *Langmuir*, 1986, **2**, 717–722.
46 M. L. Horng, J. A. Gardecki, A. Papazyan and M. Maroncelli, *J. Phys. Chem.*, 1995, **99**, 17311–17337.
47 P. Sen, D. Roy, S. K. Mondal, K. Sahu, S. Ghosh and K. Bhattacharyya, *J. Phys. Chem. A*, 2005, **109**, 9716–9722.
48 M. Ferrer and P. Lianos, *Langmuir*, 1996, **12**, 5620–5624.
49 G. Durgun, K. Ocakoglu and S. Ozcelik, *J. Phys. Chem. C*, 2011, **115**, 16322–16332.
50 S. Santra, B. Liesenfeld, C. Bertolino, D. Dutta, Z. Cao, W. Tan, B. M. Moudgil and R. A. Mericle, *J. Lumin.*, 2006, **117**, 75–82.
51 A. Huntsman International LLC, http://www.huntsman.com/performance_products/a/Products.

